Near-Optimal Distributed Band-Joins through Recursive Partitioning

Rundong Li*
Google, USA
eadon.lee@gmail.com

Wolfgang Gatterbauer
Northeastern University, USA
w.gatterbauer@northeastern.edu

Mirek Riedewald
Northeastern University, USA
m.riedewald@northeastern.edu

ABSTRACT

We consider running-time optimization for band-joins in a distributed system, e.g., the cloud. To balance load across worker machines, input has to be partitioned, which causes duplication. We explore how to resolve this tension between *maximum load per worker* and *input duplication* for band-joins between two relations. Previous work suffered from high optimization cost or considered partitionings that were too restricted (resulting in suboptimal join performance). Our main insight is that *recursive partitioning of the join-attribute space* with the appropriate split scoring measure can achieve both low optimization cost and low join cost. It is the first approach that is not only effective for one-dimensional band-joins but also for joins on multiple attributes. Experiments indicate that our method is able to find partitionings that are within 10% of the *lower bound* for both maximum load per worker and input duplication for a broad range of settings, significantly improving over previous work.

CCS CONCEPTS

• **Information systems** → **MapReduce-based systems**; *Relational parallel and distributed DBMSs.*

KEYWORDS

band-join; distributed joins; running-time optimization

ACM Reference Format:
Rundong Li, Wolfgang Gatterbauer, and Mirek Riedewald. 2020. Near-Optimal Distributed Band-Joins through Recursive Partitioning. In *Proceedings of the 2020 ACM SIGMOD International Conference on Management of Data (SIGMOD'20), June 14–19, 2020, Portland, OR, USA.* ACM, New York, NY, USA, 16 pages. https://doi.org/10.1145/3318464.3389750

*Work performed while PhD student at Northeastern University.

SIGMOD'20, June 14–19, 2020, Portland, OR, USA

ACM ISBN 978-1-4503-6735-6/20/06…$15.00
https://doi.org/10.1145/3318464.3389750

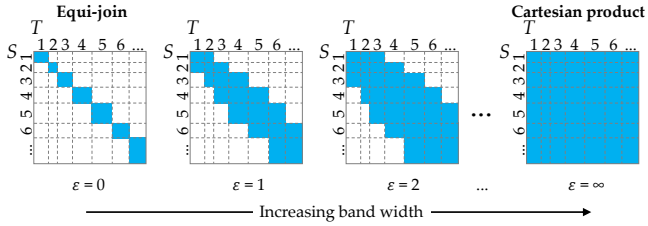

Figure 1: Join matrices for one-dimensional (1D) band-join $|S.A - T.A| \leq \varepsilon$ for increasing band width ε from equi-join ($\varepsilon = 0$) to Cartesian product ($\varepsilon = \infty$). Numbers on matrix rows and columns indicate distinct A-values of input tuples. Cell (i, j) corresponds to attribute pair (s_i, t_j) and is shaded iff the pair fulfills the join condition and is in the output.

1 INTRODUCTION

Given two relations S and T, the band-join $S \bowtie_B T$ returns all pairs $(s \in S, t \in T)$ that are "close" to each other. Closeness is determined based on band-width constraints on the join attributes which we also call *dimensions*. This is related to (but in some aspects more general than, and in others a special case of) *similarity joins* (see Section 3). The Oracle Database SQL Language Reference guide [23] presents a one-dimensional (1D) example of a query finding employees whose salaries differ by at most $100. Their discussion of band-join specific optimizations highlights the operator's importance. Zhao et al [45] describe an astronomy application where celestial objects are matched using band conditions on time and coordinates *ra* (right ascension) and *dec* (declination). This type of approximate matching based on space and time is very common in practice and leads to three-dimensional (3D) band-joins like this:

Example 1. *Consider bird-observation table* `B` *with columns* `longitude`, `latitude`, `time`, `species`, `count`, *and weather table* `W`, *reporting precipitation and temperature for location-time combinations. A scientist studying how weather affects bird sightings wants to join these tables on attributes* `longitude`, `latitude`, *and* `time`. *Since weather reports do not cover the exact time and location of the bird sighting, she uses a band-join to link each bird report with weather data for "nearby" time and location, e.g.,* `|B.longitude − W.longitude| ≤ 0.5 AND |B.latitude − W.latitude| ≤ 0.5 AND |B.time − W.time| ≤ 10`.

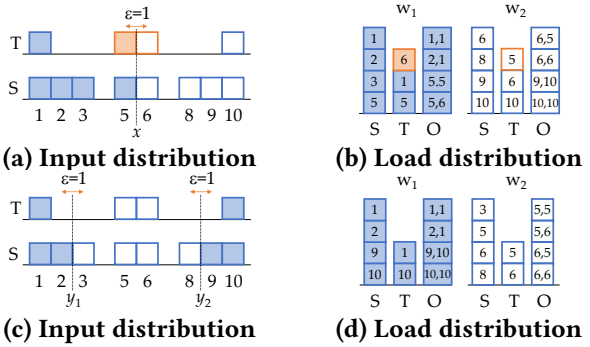

Figure 2: Input (S, T) and output (O) on workers w_1 and w_2 when splitting on x (top row). The T-tuples shown in orange are duplicated because they are within the band width of the split point. When splitting on y_1 and y_2, no tuple is duplicated and load is perfectly balanced (bottom row).

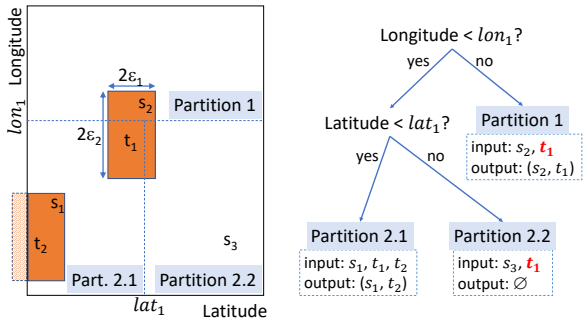

Figure 3: Recursive *split tree* for a 2D band-join on latitude and longitude. All splits are T-splits, i.e., T-tuples within band width of the split boundary are sent to both children. For instance, at the root the ε-range (orange box) of t_1 crosses the lon_1 line and therefore the tuple is copied to the right sub-tree (partition 1). The same happens again for the split on lat_1. This ensures that no match is missed (e.g., (s_2, t_1)) and no output tuple is produced twice.

We are interested in minimizing end-to-end running time of distributed band-joins, which is the sum of (1) *optimization time* (for finding a good execution strategy) and (2) *join time* (for the join execution). Join time depends on the *data partitioning* used to assign input records to worker machines. As seen in Figure 1, band-joins generalize equi-join and Cartesian product. Partitioning algorithms with optimality guarantees are known only for these two extremes [1, 26, 29].

Example 2. *To see why distributed band-joins are difficult, consider a 1D join with band width $\varepsilon = 1$ of $S = \{1, 2, 3, 5, 6, 8, 9, 10\}$ and $T = \{1, 5, 6, 10\}$ on $w = 2$ workers. For balancing load, we may split S on value x and send the left half to worker w_1 and the right half to w_2 (see Figure 2a). To not miss results near the split point, all T-tuples within band width $\varepsilon = 1$ of x have to be copied across the boundary. Figure 2b shows the resulting input and output tuples on each worker, with duplicates in orange. By splitting in sparse regions of T, e.g., on y_1 and y_2 (Figures 2c and 2d), perfect load balance can be achieved without input duplication.*

The main contribution of this work is a novel algorithm RecPart (***Rec**ursive **Part**itioning*) *that quickly and efficiently finds split points such as y_1 and y_2.* To do so, it has to carefully navigate the tradeoff between load balance and input duplication. For instance, y_1 by itself appears like a poor choice from a load-balance point of view. It takes the additional split on y_2 to unlock y_1's true potential.

Overview of the approach. We propose recursive (i.e., hierarchical) partitioning of the join-attribute space, because it offers a broad variety of partitioning options that can be explored efficiently. As illustrated by the *split tree* in Figure 3, each path from the root node to a leaf defines a partition of the join-attribute space as a conjunction of the split predicates in the nodes along the path. Like *decision trees* in machine learning [16], RecPart's split tree is grown from the root, each time recursively splitting some leaf node. This step-wise expansion is a perfect solution for the problem of *navigating two optimization goals*: minimizing max worker load and minimizing input duplication. As RecPart grows the tree, input duplication is monotonically increasing, because more tuples may have to be copied across a newly added split boundary. At the same time, large partitions are broken up and hence load balance may improve.

To find good partitionings, it is important to (1) use an appropriate scoring function to pick a good split point (e.g., choose y_1 or y_2 over x in Figure 2) and to (2) choose the best leaf to be split next. We propose the *ratio between load balance improvement and additional input duplication* for both decisions. In Example 2, this would favor y_1 and y_2 over x, because they add zero duplication. Similarly, a leaf node with a zero-duplicate split option would be preferred over a leaf whose split would cause duplication.

When a leaf becomes so small that virtually all tuples in the corresponding partition join with each other, then it is not split any further. However, if the load induced by that partition is high, then the leaf "internally" uses a grid-style partitioning inspired by 1-Bucket [29] to create more fine-grained partitions. This is motivated by the observation that the band-join computation in a sufficiently small partition behaves like a Cartesian product—for which 1-Bucket was shown to be near-optimal.

Main contributions. (1) We demonstrate analytically and empirically that previous work falls short either due to high optimization time (to find a partitioning) or due to high join time (caused by an inferior partitioning), especially for band-joins in more than one dimension.

(2) To address those shortcomings, we propose *recursive partitioning* of the multidimensional join-attribute space. Given a fixed-size input and output sample, our algorithm

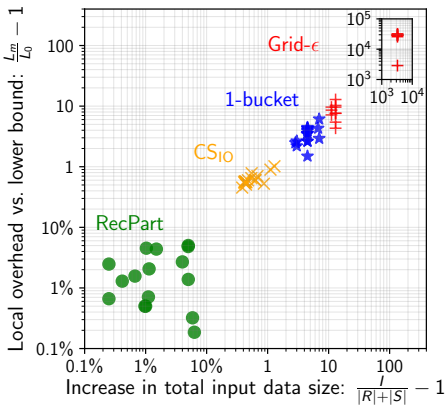

Figure 4: Total input duplication (x-axis) and maximum overhead across workers (y-axis) for a variety of data points for our method RecPart vs. 3 competitors (see Section 6 for details). RecPart is always within 10% of the lower bounds (0% duplication and 0% overhead).

RecPart finds a partitioning in $O(w \log w + wd)$, where w is the number of workers and d is the number of join attributes, i.e., the dimensionality of the band-join. RecPart is inspired by decision trees [16], which had not been explored in the context of optimizing running time of distributed band-joins. To make them work for our problem, we identify a *new scoring measure* to determine the best split points: *ratio of load variance reduction to input duplication increase*. It is informed by our observation that a good split should improve load balance with minimal additional input duplication. We also identify a *new stopping condition* for tree growth.

(3) While we could not prove near-optimality of RecPart's partitioning, our experiments provide strong empirical evidence. Across a variety of datasets, cluster sizes, and join conditions, RecPart always found partitions for which both total input duplication and max worker load were within 10% of the corresponding *lower bounds*, beating all competitors (even those with significantly higher optimization cost) by a wide margin. Figure 4 shows this for a variety of problems (notice the log scale). The definition of the axes, the algorithms, and the detailed experiments are presented in Section 2, Section 3, and Section 6, respectively.

(4) We prove new Lemmas 2 and 3 that characterize when grid partitioning will be effective for distributed band-joins.

Additional material can be found in the extended version of this article [24].

2 PROBLEM DEFINITION

Without loss of generality, let S and T be two relations with the same schema $(A_1, A_2, \ldots, A_d)$. Given a band width $\varepsilon_i \geq 0$ for each attribute A_i, the band-join of S and T is defined as

$$S \bowtie_B T = \{(s,t) : s \in S \wedge t \in T \wedge \forall_{1 \leq i \leq d} |s.A_i - t.A_i| \leq \varepsilon_i\}.$$

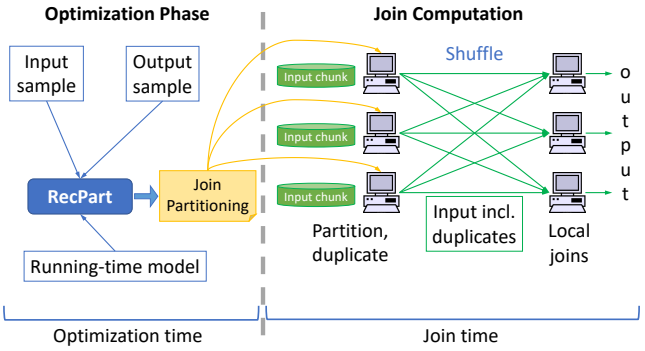

Figure 5: Overview of the proposed approach.

We call d the *dimensionality* of the join and A_i the i-th *dimension*. We refer to the d-dimensional hyper-rectangle centered around a tuple a with side-length $2\varepsilon_i$ in dimension i, formally $\{(x_1, \ldots, x_d) : \forall_{1 \leq i \leq d}\, a.A_i - \varepsilon_i \leq x_i \leq a.A_i + \varepsilon_i\}$, as the *$\varepsilon$-range* around a (depicted as an orange box in Figure 3). Note that (s,t) is in the output iff s falls into the ε-range around t (and vice versa). It is straightforward to generalize all results in this paper to asymmetric band conditions $(a.A_i - \varepsilon_{i_L} \leq x_i \leq a.A_i + \varepsilon_{i_R})$ and to relations with attributes that do not appear in the join condition.

Definition 1 (Join Partitioning). *Given input relations S and T with $Q = S \bowtie_B T$ and w worker machines. A* join partitioning *is an assignment $h : (S \cup T) \rightarrow 2^{\{1,\ldots,w\}} \setminus \emptyset$ of each input tuple to one or more workers so that each join result $q \in Q$ can be recovered by exactly one local join.*

A *local join* is the band-join executed by a worker on the input subset it receives. The definition ensures that *each output tuple is produced by exactly one worker*, which avoids an expensive post-processing phase for duplicate elimination and is in line with previous work [1, 19, 29, 39].

Given S, T, and a band-join condition, our goal is to minimize the time to compute $S \bowtie_B T$. This time is the sum of *optimization time* (i.e., the time to find a join partitioning) and *join time* (i.e., the time to compute the result based on this partitioning), as illustrated in Figure 5.

We follow common practice and define the load L_i on a worker w_i as the weighted sum $L_i = \beta_2 I_i + \beta_3 O_i$, $0 \leq \beta_2, 0 \leq \beta_3$ of input I_i and output O_i assigned to it [1, 26, 29, 39]. *Max worker load* $L_m = \max_i L_i$ is the maximum load assigned to any worker. In addition, we also evaluate a partitioning based on its *total amount of input* I. It accounts for given inputs S and T and all duplicates created by the partitioning, i.e., $I = \sum_{x \in S \cup T} |h(x)|$. Recall from Definition 1 that h assigns input tuples to a subset of the workers, i.e., $|h(x)|$ is the number of workers that receive tuple x.

Lemma 1 (Lower Bounds). *$|S| + |T|$ is a lower bound for total input I. And $L_0 = (\beta_2(|S| + |T|) + \beta_3|S \bowtie_B T|)/w$ is a lower bound for max worker load L_m.*

The lower bound for total input I follows from Definition 1, because each input tuple has to be examined by at least one worker. For max worker load, note that any partitioning has to distribute a total input of at least $|S|+|T|$ and a total output of $|S \bowtie_B T|$ over the w workers, for a total load of at least $\beta_2(|S| + |T|) + \beta_3|S \bowtie_B T|$.

System Model and Measures of Success. We consider the standard Hadoop MapReduce and Spark environment where inputs S and T are stored in files. These files may have been chunked up before the computation starts, with chunks distributed over the workers. Or they may reside in a separate cloud storage service such as Amazon's S3. The files are not pre-partitioned on the join attributes and the workers do not have advance knowledge which chunk contains which join-attribute values. Hence any desired join partitioning requires that—in MapReduce terminology—(1) the entire input is read by map tasks and (2) a full shuffle is performed to group the data according to the partitioning and have each group be processed by a reduce task.

In this setting, the shuffle time is determined by total input I, and the duration of the reduce phase (each worker performing local joins) is determined by max worker load. Hence we are interested in evaluating how close a partitioning comes to the lower bounds for total input and max worker load (Lemma 1). We use $\frac{I-(|S|+|T|)}{|S|+|T|}$ and $\frac{L_m-L_0}{L_0}$, respectively, which measure by how much a value exceeds the lower bound, relative to the lower bound. For instance, for $L_m = 11$ and $L_0 = 10$ we obtain 0.1, meaning that the max worker load of the partitioning is 10% higher than the lower bound.

For systems with very fast networks, an emerging trend [2, 34], data transfer time is negligible compared to local join time, therefore the goal is to minimize max worker load, i.e., the success measure is $\frac{L_m-L_0}{L_0}$. In applications where the input is already *pre-partitioned on the join attributes* (e.g., for dimension-dimension array joins [11]) the optimization goal concentrates on reducing data movement [45]. There our approach can be used to *find the best pre-partitioning*, i.e., to chunk up the array on the dimensions.

In addition to comparing to the lower bounds, we also measure end-to-end running time for a MapReduce/Spark implementation of the band-join in the cloud. For join-time estimation we rely on the model by Li et al. [25], which was shown to be sufficiently accurate to optimize running time of various algorithms, including equi-joins. Similar to the equi-join model, our band-join model $\mathcal{M}$ takes as input triple (I, I_m, O_m) and estimates join time as a piecewise linear model $\mathcal{M}(I, I_m, O_m) = \beta_0 + \beta_1 I + \beta_2 I_m + \beta_3 O_m$. The β-coefficients are determined using linear regression on a small benchmark of training queries and inputs.

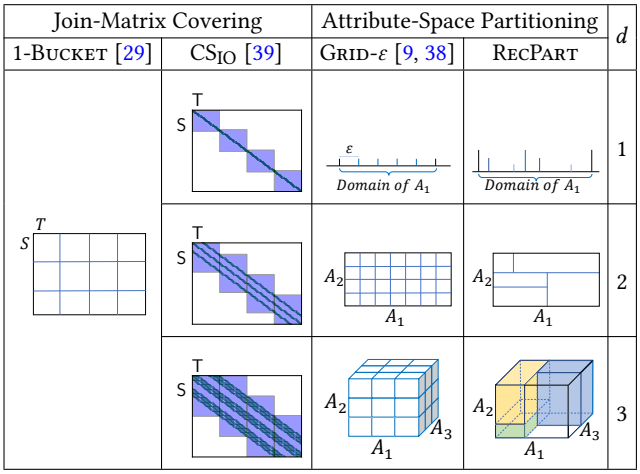

Figure 6: Illustration of partitioning methods for band-joins in d-dimensional space for $d = 1, 2, 3$; the A_i are the join attributes. Grid-ε and RecPart partition the d-dimensional *join-attribute space*, while CSIO and 1-Bucket create partitions by finding a cover of the 2-dimensional *join matrix* $S \times T$, whose dimensions are independent of the dimensionality of the join condition. Bar height for RecPart and $d = 1$ indicates recursive partition order.

3 RELATED WORK

3.1 Direct Competitors

Direct competitors are approaches that (1) support distributed band-joins and (2) optimize for load balance, i.e., max worker load or a similar measure. We classify them into *join-matrix covering* vs *attribute-space partitioning*.

Join-matrix covering. These approaches model distributed join computation as a covering problem for the *join matrix* $J = S \times T$, whose rows correspond to S-tuples and columns to T-tuples. A cell $J(s, t)$ is "relevant" iff (s, t) satisfies the join condition. Any theta-join, including band-joins, can be represented as the corresponding set of relevant cells in J. A join partitioning can then be obtained by covering all relevant cells with non-overlapping regions. Since the exact set of relevant cells is not known a priori (it corresponds to the to-be-computed output), the algorithm covers a larger region of the matrix that is guaranteed to contain all relevant cells. For instance, for inequality predicates, M-Bucket-I [29] partitions both inputs on approximate quantiles in one dimension and then covers with w rectangles all regions corresponding to combinations of inter-quantile ranges from S and T that could potentially contain relevant cells. IEJoin [19] directly uses the same quantile-based range partitioning, but without attempting to find a w-rectangle cover. Its main contribution is a clever *in-memory* algorithm for queries with two join predicates. Optimizing local processing is orthogonal to our focus on how to *assign input*

tuples to multiple workers. In fact, one can use an adaptation of their idea for local band-join computation on each worker.

To support any theta-join, 1-Bucket [29] covers the entire join matrix with a grid of r rows and c columns. This is illustrated for $r = 3$ and $c = 4$ in Figure 6. Each S-tuple is randomly assigned to one of the r rows (which implies that it is sent to *all* c partitions in this row); this process is analogous for T-tuples, which are assigned to random columns. While randomization achieves near-perfect load balance, input is duplicated approximately $\sqrt{w}$ times.

Zhang et al. [44] extend 1-Bucket to joins between many relations. Koumarelas et al. [22] explore re-ordering of join-matrix rows and columns to improve the running time of M-Bucket-I [29]. However, like M-Bucket-I, their technique does not take output distribution into account. This was shown to lead to poor partitionings by Vitorovic et al. [39] whose method CS_{IO} represents the state of the art for distributed theta-joins. It relies on a carefully tuned optimization pipeline that first range-partitions S and T using approximate quantiles, then coarsens those partitions, and finally finds the optimal (in terms of max worker load) rectangle covering of the coarsened matrix. The resulting partitioning was shown to be superior—including for band-joins—to direct quantile-based partitioning, which is used by IEJoin. Figure 6 illustrates CS_{IO} for a covering with four rectangles for 1, 2 and 3 dimensions. The darker diagonal "bands" show relevant matrix cells, i.e., cells that have to be covered. Notice how join dimensionality affects relevant-cell locations, but does not affect the dimensionality of the join matrix: *for a join between two input relations S and T, the join matrix is always two-dimensional, with one dimension per input relation.*

CS_{IO} suffers from high optimization cost to find the covering rectangles, which uses a tiling algorithm of complexity $O(n^5 \log n)$ for n input tuples. Optimization cost can be reduced by coarsening the statistics used. Further reduction in optimization cost is achieved for monotonic join matrices, a property that holds for 1-dimensional band-joins but *not for multidimensional ones*. As our experiments will show, the high optimization cost hampers the approach for multidimensional band-joins.

Attribute-space partitioning. Instead of using the 2-dimensional $S \times T$ join matrix, attribute-space partitioning works in the d-dimensional space $A_1 \times A_2 \times \cdots \times A_d$ defined by the domains of the join attributes. Grid partitioning of the attribute space was explored in the early days of parallel databases, yet only for one-dimensional conditions. Soloviev [38] proposes the *truncating hash algorithm* and shows that it improves over a parallel implementation of the hybrid partitioned band-join algorithm by DeWitt et al. [9]. The method generalizes to more dimensions as illustrated in the Grid-ε column in Figure 6. Grid cells define partitions and are assigned to the workers.

By default, Grid-ε sets grid size for attribute A_i to the band width ε_i in that dimension. This results in near-zero optimization cost, but may create a poor load balance (for skewed input) and high input duplication (when a partition boundary cuts through a dense region). A coarser grid reduces input duplication, but the larger partitions make load balancing more challenging. Our approach RecPart, which also applies attribute-space partitioning, mitigates the problem by considering recursive partitionings that avoid cutting through dense regions.

3.2 Other Related Work

Similarity joins are related to band-joins, but neither generalizes the other: the similarity joins closest to band-joins define a pair $(s \in S, t \in T)$ as similar if $\text{sim}(s, t) > \theta$, for some similarity function sim and threshold θ. This includes *1D* band-joins as a special case, but does not support band-joins in multiple dimensions. (A band-join in d dimensions has $2d$ threshold parameters for lower and upper limits in each dimension.) A recent survey [13] compares 10 distributed set-similarity join algorithms. The main focus of previous work on similarity joins is on addressing the specific challenges posed by working in a *general metric space* where vector-space operations such as addition and scalar multiplication (which band-joins can exploit) are not available. A particular focus is on (1) identifying fast filters that prune away a large fraction of candidate pairs without computing their similarity and (2) selecting pivot elements or anchor points to form partitions, e.g., via sampling [35].

Duggan et al [11] study skew-aware optimization for **distributed array equi-joins** (not band-joins). The work by Zhao et al [45] is closest to ours, because they introduce array similarity joins that can encode multi-dimensional band-join conditions. However, it is not a direct competitor for RecPart, because it considers a different optimization problem: The array is assumed to be already grid-partitioned into chunks on the join attributes and the main challenge is to co-locate with minimal network cost those partitions that need to be joined. Our approach is orthogonal for two reasons: First, we do not make any assumptions about existing pre-partitioning on the join attributes and hence the join requires a full data shuffle. Second, we show that for band-joins, grid partitioning is inferior to RecPart's recursive partitioning. Hence RecPart provides new insights for choosing better array partitions when the array DBMS anticipates band-join queries.

Attribute-space partitioning is explored in other contexts for optimization goals that are very different from distributed band-join optimization. For array tiling, the goal is to minimize page accesses of range queries [14]. Here, like

Algorithm 1: RecPart

Data: S, T, band-join condition, sample size k
Result: Hierarchical partitioning $\mathcal{P}^*$ of $A_1 \times \cdots \times A_d$

Draw random input sample of size $k/2$ from S and T
Draw random output sample [39] of size up to $k/2$
Initialize $\mathcal{P}$ with root partition $p_r = A_1 \times \cdots \times A_d$
p_r.(bestSplit, topScore) = best_split(p_r)
repeat
  Let $p \in \mathcal{P}$ be the leaf node with the highest topScore
  Apply p.bestSplit
  foreach *newly created (for regular leaf split) or updated (for small leaf split) leaf node* p' **do**
    p'.(bestSplit, topScore) = best_split(p')
until *termination condition*
Return best partitioning $\mathcal{P}^*$ found

for histogram construction [32, 33], the band-join's data duplication across a split boundary is not taken into account. Histogram techniques optimize for a different goal: maximizing the information captured with a given number of partitions. Only the equi-weight histograms by Vitorovic et al. [39] take input duplication into account. We include their approach CS_{IO} in our comparison.

For equi-joins, several algorithms address skew by **partitioning heavy hitters** [1, 4, 10, 27, 30, 31, 41, 42]. Other than the high-level idea of splitting up large partitions to improve load balance, the concrete approaches do not carry over to band-joins: They rely on the property that tuples with different join values cannot be matched, i.e., do not capture that tuples within band width of a split boundary must be duplicated. However, our decision to use load variance for measuring load balance was inspired by the state-of-the-art equi-join algorithm of Li et al. [26]. Earlier work relied on hash partitioning [8, 21] and focused on assigning partitions to processors [7, 12, 17, 18, 20, 34, 40]. Empirical studies of parallel and distributed equi-joins include [3, 5, 8, 36, 37].

4 RECURSIVE PARTITIONING

We introduce RecPart and analyze its complexity.

4.1 Main Structure of the Algorithm

RecPart (Algorithm 1) is inspired by decision trees [16] and recursively partitions the d-dimensional space spanned by all join attributes. To adapt this high-level idea to running-time optimization for band-joins, we (1) identify a new split-scoring measure that determines the selection of split boundaries, (2) propose a new stopping condition for the splitting process, and (3) propose an ordering to determine which tree leaf to consider next for splitting. The splitting process is illustrated in Figure 7.

Algorithm 2: best_split

Data: Partition p, input and output sample tuples in p, number of row sub-partitions r and column sub-partitions c ($r = c = 1$ for regular partitions)
Result: Split predicate bestSplit and its score topScore

Initialize topScore = 0 and bestSplit = NULL
if *p is a regular partition* **then**
  `// Find best decision-tree style split`
  foreach *regular dimension* A_i **do**
    Let x_i be the split predicate on dimension A_i that has the highest ratio $\sigma_i = \Delta\text{Var}(x_i)/\Delta\text{Dup}(x_i)$ among all possible splits in dimension A_i
    if $\sigma_i >$ topScore **then**
      Set topScore = σ_i and set bestSplit = x_i
else
  `// Small partition: increment number of row or column sub-partitions using 1-Bucket`
  Let $\sigma_r = \Delta\text{Var}(r+1, c)/\Delta\text{Dup}(r+1, c)$
  Let $\sigma_c = \Delta\text{Var}(r, c+1)/\Delta\text{Dup}(r, c+1)$
  if $\sigma_r > \sigma_c$ **then**
    Set topScore = σ_r and set bestSplit = row
  else
    Set topScore = σ_c and set bestSplit = column
Return (bestSplit, topScore)

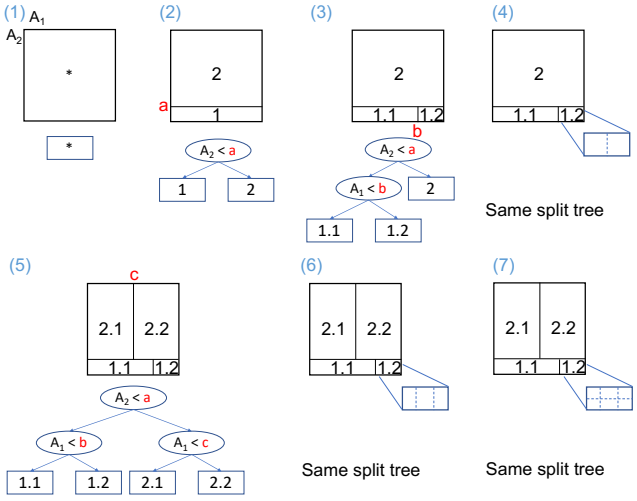

Figure 7: Recursive partitioning for a 2D band-join on attributes A_1 and A_2. In the split tree, a path from the root to a leaf defines a rectangular partition in $A_1 \times A_2$ as the conjunction of all predicates along the path. (By convention the left child is the branch satisfying the split predicate.) In small partitions such as 1.2, RecPart applies 1-Bucket. Those partitions are terminal leaves in the split tree and only change their "internal" partitioning.

Algorithm 1 starts with a single leaf node covering the entire join-attribute space and calls best_split (Algorithm 2)

on this leaf to find the best possible split and its score. Assuming the leaf is a "regular" partition (we discuss small partitions below), best_split sorts the input sample on A_1 and tries all middle-points between consecutive A_1-values as possible split boundaries. Then it does the same for A_2. *The winning split boundary is the one with the highest ratio between load-variance reduction and input duplication increase* (see details in Section 4.2).

Assume the best split is $A_2 < a$. The first execution of the repeat-loop then applies this split, creating new leaves "1" and "2" and finding the best split for each of them. Which leaf should be split next? *RecPart manages all split-tree leaves in a priority queue based on their* topScore *value.* Assuming leaf "1" has the higher score, the next repeat-loop iteration will split it, creating new leaves "1.1" and "1.2". This process continues until the appropriate termination condition is reached (discussed below). As the split tree is grown, the algorithm also keeps track of the best partitioning found so far.

4.2 Algorithm Details

Small partitions. When a partition becomes "small" relative to band width in a dimension, then no further *recursive* splitting in that dimension is allowed. When the partition is small in *all* dimensions, then it switches into a different partitioning mode inspired by 1-Bucket [29]. This is motivated by the observation that when the length of a partition approaches band width in each dimension, then all S and T-tuples in that partition join with each other. And for Cartesian products, 1-Bucket was shown to be near-optimal.

We define a partition as "small" as soon as its size is below twice the band width in all dimensions. In Figure 7 step (4), leaf "1.2" is small and hence when it is picked in the repeat-loop, applying the best split leaves the split tree unchanged, but instead increases the number of column partitions c to 2. Afterward, the topScore value of leaf "1.2" may have decreased and leaf "2" is split next, using a regular recursive split. This may be followed by more "internal" splits of leaf "1.2" in later iterations as shown in Figure 7, steps (6) and (7).

It is easy to show that having some leaves in "regular" and others in "small" split mode does not affect correctness. Intuitively, this is guaranteed because duplication only needs to be considered inside the region that is further partitioned, i.e., it does not "bleed" beyond partition boundaries.

Split scoring. In split score $\Delta\text{Var}(x_i)/\Delta\text{Dup}(x_i)$ for a regular dimension (Algorithm 2), $\Delta\text{Var}(x_i)$ is defined as follows: Let $\mathcal{L}$ denote the set of split-tree leaves. Each (sub-partition in a) leaf corresponds to a region p in $A_1 \times \cdots \times A_d$, for which we estimate input I_p and output O_p from the random samples drawn by Algorithm 1. The load induced by p is $l_p = \beta_2 I_p + \beta_3 O_p$. Load variance is computed as follows: Assign each leaf in $\mathcal{L}$ to a randomly selected worker. Then per-worker load is a random variable $\mathcal{P}$ (we slightly abuse notation to avoid notational clutter) whose variance can be shown to be $\mathbb{V}[\mathcal{P}] = \frac{w-1}{w^2} \sum_{p \in \mathcal{L}} l_p^2$. We analogously obtain $\mathbb{V}(\mathcal{P}')$ for a partitioning $\mathcal{P}'$ that results from splitting some leaf $p' \in \mathcal{L}$ into sub-partitions p_1 and p_2 using predicate x_i. Then $\Delta\mathbb{V}(x_i) = \mathbb{V}(\mathcal{P}') - \mathbb{V}(\mathcal{P})$. $\mathbb{V}(\mathcal{P}')$ can be computed from $\mathbb{V}(\mathcal{P})$ in *constant* time by subtracting $\frac{w-1}{w^2} l_{p'}$ and adding $\frac{w-1}{w^2}(l_{p_1} + l_{p_2})$.

The additional duplication caused by a split is obtained by estimating the number of T-tuples within band width of the new split boundary using the input sample. When multiple split predicates cause no input duplication, then the best split is the one with the greatest variance reduction among them. The calculation of load variance and input duplication for "small" leaves is analogous.

The split score reflects our goal of reducing max worker load with minimal input duplication. For the former, load-variance reduction could be replaced by other measures, but precise estimation of input and output on the most loaded worker is difficult due to dynamic load balancing applied by schedulers at runtime. We therefore selected load variance as a scheduler-independent proxy.

Termination condition and winning partitioning. We propose a *theoretical* and an *applied* termination condition for the repeat-loop in Algorithm 1. For the theoretical approach, the winning partitioning is the one with the *lowest overhead over the lower bound in terms of both max worker load and input duplication*, i.e., the one with the minimal value of $\max\left\{\frac{I-(|S|+|T|)}{|S|+|T|}; \frac{L_m-L_0}{L_0}\right\}$. It is easy to show that each iteration of the repeat-loop monotonically increases input I, because each new split boundary (regular leaf) and more fine-grained sub-partitioning (small leaf) can only increase the number of input duplicates. At the same time, the loop iteration may or may not decrease $\frac{L_m-L_0}{L_0}$. Hence repeat-loop iterations can be terminated as soon as $\frac{I-(|S|+|T|)}{|S|+|T|}$ exceeds the smallest value of $\frac{L_m-L_0}{L_0}$ encountered so far.

The theoretical approach only needs input and output samples, as well as an estimate of the relative impact of an input tuple versus an output tuple on local join computation time. Input sampling is straightforward; for output sampling we use the method from [39]. If the output is large, it efficiently produces a large sample. If the output is small, then the output has negligible impact on join computation cost. The experiments show that we get good results when limiting sample size based on memory size and sampling cost to at most 5% of join time.

For estimating load impact, we run band-joins with different input and output sizes I and O on an individual worker and use linear regression to determine β_2 and β_3 in load function $\beta_2 I + \beta_3 O$. In our Amazon cloud cluster, $\beta_2/\beta_3 \approx 4$. Note that β_2 and β_3 tend to increase with input and output. For the

lower bound, we use the smallest values, i.e., those obtained for scenarios where a node receives about $1/w$ of the input (recall that w is the number of workers). This establishes a lower value for the lower bound, i.e., it is more challenging for RecPart to be close to it.

For the applied approach, we use the cost model as discussed in the end of Section 2. The winning partitioning is the one with the lowest running time predicted by the cost model. Repeat-loop iterations terminate when estimated join time bottoms out. We detect this based on a window of the join times over the last w repeat-loop iterations: loop execution terminates when improvement is below 1% (or join time even increased) over those last w iterations. (We chose w as window size because it would take at least one extra split per worker to break up each worker's load. This dovetails with the prioritization of leaves: The most promising leaves in terms of splitting up load with low input duplication overhead are greedily selected.)

Extension: symmetric partitioning. Like classic grid partitioning, RecPart as discussed so far treats inputs S and T differently: at an inner node in the split tree, S is partitioned (without duplication), while T-tuples near the split boundary are duplicated. For regions where S is sparse and T is dense, we want to reverse these roles. Consider Figure 2c, where y_1 and y_2 enabled a zero-duplication partitioning with perfect load balance. What if the input distribution was reversed in another region of the join-attribute space, e.g., $S' = \{21, 25, 26, 30\}$ and $T' = \{21, 22, 23, 25, 26, 28, 29, 30\}$? Then no split in range 21 to 30 could avoid duplication of T'-tuples because for band width 1 at least one of the T'-values would be within 1 of the split point. In that scenario we want to reverse the roles of S' and T', i.e., perform the partitioning on T' and the partition/duplication on S'.

For grid partitioning, it is not clear how to reverse the roles of S and T in some of the grid cells. For RecPart, this turns out to be easy. When exploring split options in a regular leaf (1-Bucket in small partitions already treats both inputs symmetrically), Algorithm 2 computes the duplication for both cases: partition S and partition/duplicate T as well as the other way round. We call the former a *T-split* and the latter an *S-split*. The split type information is added to the corresponding node in the split tree.

Algorithm 3 is used to determine which tuples to assign to the sub-trees. (Only the version for T-tuples is shown; the one for S-tuples is analogous.) It is easy to show that for each result $(s, t) \in S \bowtie_B T$, exactly one leaf in the split tree receives both s and t.

Algorithm 3: assign_input

Data: Input tuple $t \in T$; node p in split tree
Result: Set of leaves to which t is copied

```
1 if p is a leaf then
2 |  Return (1-Bucket (t, p))
3 else
4 |  if p is a T-split node then
5 |  |  for each child partition p' of p that intersects with the
  |  |    ε-range of t do
6 |  |  |  assign_input(t, p')
7 |  else
8 |  |  Let p' be the child partition of p that contains t
9 |  |  assign_input(t, p')
```

4.3 Algorithm Analysis

RecPart has low complexity, resulting in low optimization time. Let λ denote the number of repeat-loop executions in Algorithm 1. Each iteration increases the number of leaves in the split tree by at most one. The algorithm manages all leaves in a priority queue based on the score returned by Algorithm 2. With a priority queue where inserts have constant cost and removal of the top element takes time logarithmic in queue size, an iteration of the repeat-loop takes $O(\log \lambda)$ to remove the top-scoring leaf p. If p is regular, then it takes $O(1)$ to create sub-partitions p_1 and p_2 and to distribute all input and output samples in p over them. (Sample size is bounded by constant k, a fraction of machine-memory size.) Checking if p_1 and p_2 are small partitions takes time $O(d)$. Then best_split is executed, which for a regular leaf requires sorting of the input sample on each dimension and trying all possible split points, each a middle point between two consecutive sample tuples in that dimension. Since sample size is upper-bounded by a constant, the cost is $O(d)$. For a small leaf, the cost is $O(1)$. Finally, inserting p_1 and p_2 into the priority queue takes $O(1)$. In total, splitting a regular or small leaf has complexity $O(d)$ and $O(1)$, respectively.

After λ executions of the repeat-loop in Algorithm 1, the next iteration has complexity $O(\log \lambda + d)$. Hence the total cost of λ iterations is $O(\lambda \log \lambda + \lambda d)$. In our experience, the algorithm will terminate after a number of iterations bounded by a small multiple of the number of worker machines. To see why, note that each iteration breaks up a large partition p and replaces it by two (for regular p) or more (for small p) sub-partitions. The split-scoring metric favors breaking up heavy partitions, therefore load can be balanced across workers fairly evenly as soon as the total number of partitions reaches a small multiple of the number of workers. This in turn implies for Algorithm 1, given samples of fixed size, a total complexity of $O(w \log w + wd)$.

5 ANALYTICAL INSIGHTS

We present two surprising results about the ability of grid partitioning to address load imbalances. For join-matrix covering approaches like CS_{IO} that depend on the notion of a

total ordering of the join-attribute space, we explore how to enumerate the multi-dimensional space.

5.1 Properties of Grid Partitioning

Without loss of generality, let S be the input that is partitioned and T be the input that is partitioned/duplicated.

Input duplication. With grid-size in each dimension set to the corresponding band width, the ε-range of a T-tuple intersects with up to 3 grid cells per dimension, for a total replication rate of $O(3^d)$ in d dimensions. Can this exponential dependency on the dimensionality be addressed through coarser partitioning? Unfortunately, for any non-trivial partitioning, asymptotically the replication rate is still at least $O(2^d)$. To construct the worst case, an adversary places all input tuples near the corner of a centrally located grid cell.

Max worker load. We now show an even stronger negative result, indicating that grid-partitioning is inherently limited in its ability to reduce max worker load, no matter the number of workers or the grid size. Consider a partitioning where one of the grid cells contains half of S and half of T. Does there exist a more fine-grained grid partitioning where none of the grid cells receives more than 10% of S and 10% of T? One may be tempted to answer in the affirmative: just keep decreasing grid size in all dimensions until the target is reached. Unfortunately, this does not hold as we show next.

Lemma 2. *If there exists an ε-range in the join-attribute space with n tuples from T, then grid partitioning will create a partition with at least n T-tuples,* no matter the grid size.

Proof. For $d = 1$ consider an interval of size ε_1 that contains n T-tuples. If no split point partitions the interval, then the partition containing it has all n T-tuples. Otherwise, i.e., if at least one split point partitions the interval, pick one of the split points inside the interval, say X, and consider the T-tuples copied to the grid cells adjacent to X. Since all T-tuples in an interval of size ε_1 are within ε_1 of X, both grid cells receive all n T-tuples from the interval. It is straightforward to generalize this analysis to $d > 1$. □

In short, even though a more fine-grained partitioning can split S into ever smaller pieces, the same is not possible for T because of the duplication needed to ensure correctness for a band-join. For *skewed* input, n in Lemma 2 can be $O(|T|)$. Interestingly, we now show that grid partitioning can behave well in terms of load distribution for skewed input, as long as the input is "sufficiently" large.

Lemma 3. *Let $c_0 > 0$ be a constant such that $|S \bowtie_B T| \leq c_0(|S|+|T|)$. Let R (R') denote the region of size $\varepsilon_1 \times \varepsilon_2 \times \cdots \times \varepsilon_d$ in the join attribute space containing the most tuples from S (T); and let x (x') and y (y') denote the fraction of tuples from S and T, respectively, it contains. If there exist constants $0 < c_1 \leq c_2$ such that $c_1 \leq x/y \leq c_2$ and $c_1 \leq x'/y' \leq c_2$, then no region of size $\varepsilon_1 \times \varepsilon_2 \times \cdots \times \varepsilon_d$ contains more than $O(\sqrt{1/|S| + 1/|T|})$ input tuples.*

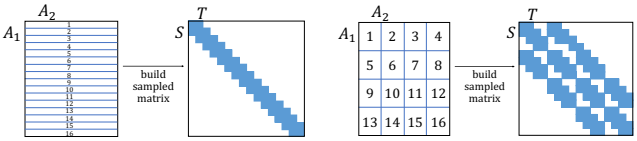

(a) Row-major order **(b) Block-style order**

Figure 8: Impact of enumeration order of a multidimensional space, here for a band-join between S and T on attributes A_1 and A_2, on the location of cells in the join matrix that may produce output. Here band width is smaller than the height and width of each partition, resulting in a significantly sparser join matrix for row-major order.

Proof. By definition, all S and T tuples in region R join with each other. Together with $|S \bowtie_B T| \leq c_0(|S| + |T|)$ this implies

$$x|S| \cdot y|T| \leq c_0(|S| + |T|) \quad \Rightarrow \quad xy \leq c_0(1/|S| + 1/|T|) \quad (1)$$

From $x/y \leq c_2$ follows $x^2 \leq c_2 xy$, then $x^2 \leq c_2 c_0(1/|S| + 1/|T|)$ (from (1)) and thus $x \leq \sqrt{c_0 c_2}\sqrt{1/|S| + 1/|T|} = O(\sqrt{1/|S| + 1/|T|})$. We show analogously for region R' that $y' \leq \sqrt{c_0/c_1}\sqrt{1/|S| + 1/|T|} = O(\sqrt{1/|S| + 1/|T|})$.

Since R is the region of size $\varepsilon_1 \times \varepsilon_2 \times \cdots \times \varepsilon_d$ with most S-tuples and R' the region with most T-tuples, no region of size $\varepsilon_1 \times \varepsilon_2 \times \cdots \times \varepsilon_d$ can contain more than x fraction of S-tuples and y' fraction of T-tuples. □

Lemma 3 is surprising. It states that for larger inputs S and T, the *fraction* of S and T in any partition of Grid-ε (recall that its partitions are of size $\varepsilon_1 \times \varepsilon_2 \times \cdots \times \varepsilon_d$) is upper-bounded by a function that decreases proportionally with $\sqrt{|S|}$ and $\sqrt{|T|}$. For instance, when S and T double in size, then the upper bound on the input fraction in any partition decreases by a factor of $\sqrt{2} \approx 1.4$.

Clearly, this does not hold for all band joins. The proof of Lemma 3 required (1) that the region with most S-tuples contain a sufficiently large fraction of T, and vice versa; and (2) that output size is bounded by c_0 times input size. The former is satisfied when S and T have a similar distribution in join-attribute space, e.g., a self-join. For the latter, we are aware of two scenarios. First, the user may actively try to avoid huge outputs by setting a smaller band width. Second, for any output-cost-dominated theta-join, 1-Bucket was shown to be near-optimal [29]. Hence specialized band-join solutions such as RecPart, Grid-ε, and CS_{IO} would only be considered when output is "sufficiently" small.

5.2 Ranges in Multidimensional Space

CS_{IO} starts with a range partitioning of the join-attribute space based on approximate quantiles. For quantiles to be

well-defined, a total order must be established on the multi-dimensional space—this was left unspecified for CS_{IO}. The ordering can significantly impact performance as illustrated in Figure 8 for a 2D band-join. In row-major order, ranges correspond to long horizontal stripes. Alternatively, each range may correspond to a "block," creating more square-shaped regions. This choice affects the candidate regions in the join matrix that need to be covered. Assume each horizontal stripe in Figure 8a is at least ε_1 high. Then an S-tuple in stripe i can only join with T-tuples in the three stripes $i-1$, i, and $i+1$. This creates the compact candidate-region diagonal of width 3 in the join matrix. For the block partitioning in Figure 8b, S-tuples in a block may join with T-tuples in up to nine neighboring blocks. This creates the wider band in the join matrix. For CS_{IO}, a wider diagonal and denser matrix cause additional input duplication.

In general, the number of candidate cells in the join matrix is minimized by row-major ordering, *if the distance between the hyperplanes in the most significant dimension is greater than or equal to the band width in that dimension.* This was the case in our experiments and therefore row-major ordering was selected for CS_{IO}.

Table 1: Band-join characteristics used in the experiments. Input and output size are reported in [million tuples].

Data Set	d	Band width	Input Size	Output Size
pareto-1.5	1	0	400	2430
pareto-1.5	1	10^{-5}	400	4580
pareto-1.5	1	$2 \cdot 10^{-5}$	400	9120
pareto-1.5	1	$3 \cdot 10^{-5}$	400	11280
pareto-1.5	3	(0, 0, 0)	400	0
pareto-1.5	3	(2, 2, 2)	400	1120
pareto-1.5	3	(4, 4, 4)	400	8740
pareto-0.5	3	(2, 2, 2)	400	12
pareto-1.0	3	(2, 2, 2)	400	420
pareto-2.0	3	(2, 2, 2)	400	3200
pareto-1.5	8	(20, . . . , 20)	100	9
pareto-1.5	8	(20, . . . , 20)	200	57
pareto-1.5	8	(20, . . . , 20)	400	219
pareto-1.5	8	(20, . . . , 20)	800	857
rv-pareto-1.5	1	2	400	0
rv-pareto-1.5	1	1000	400	0
rv-pareto-1.5	3	(1000, 1000, 1000)	400	0
rv-pareto-1.5	3	(2000, 2000, 2000)	400	0
ebird and cloud	3	(0, 0, 0)	890	0
ebird and cloud	3	(1, 1, 1)	890	320
ebird and cloud	3	(2, 2, 2)	890	2134
ebird and cloud	3	(4, 4, 4)	890	16998

6 EXPERIMENTS

We compare the total running time (optimization plus join time) of RecPart to the state of the art (Grid-ε, CS_{IO}, 1-Bucket). Note that Grid-ε is not defined for band width zero. Reported times are measured on a real cloud, unless stated otherwise. In large tables, we mark cells with the main results in blue; red color highlights a weak spot, e.g., excessive optimization time or input duplication.

6.1 Experimental Setup

Environments. Both MapReduce [6] and Spark [43] are well-suited for band-join implementation. Spark's ability to keep large data in memory makes little difference for the map-shuffle-reduce pipeline of a band-join, therefore we use MapReduce, where it is easier to control low-level behavior such as custom data partitioning. All experiments were conducted on Amazon's Elastic MapReduce (EMR) cloud, using 30 `m3.xlarge` machines (15GB RAM, 40GB disk, high network performance) by default. All clusters run Hadoop 2.8.4 with the YARN scheduler in default configuration.

Data. For synthetic data, we use a Pareto distribution where join-attribute value x is drawn from domain $[1.0, \infty)$ of real numbers and follows PDF z/x^{z+1} (greater z creates more skew). This models the famous power-law distribution observed in many real-world contexts, including the 80-20 rule for $z = \log_4 5 \approx 1.16$. We explore z in the range $[0.5, 2.0]$, which covers power-law distributions observed in real data. `pareto-`z denotes a pair of tables, each with 200 million tuples, with Pareto-distributed join attributes for skew z. High-frequency values in S are also high-frequency values in T. `rv-pareto-`z is the same as `pareto-`z, but high-frequency values in S have low frequency in T, and vice versa. Specifically, T follows a Pareto distribution from 10^6 down to $-\infty$. (T is skewed toward larger values. We generate T by drawing numbers from $[1.0, \infty)$ following Pareto distribution and then converting each number y to $10^6 - y$.)

`cloud` is a real dataset containing 382 million cloud reports [15], each reporting time, latitude, longitude, and 25 weather attributes. `ebird` is a real dataset containing 508 million bird sightings, each with attributes describing time, latitude, longitude, species observed, and 1655 features of the observation site [28].

For each input, we explore different band widths as summarized in Table 1. *Output sizes below 0.5 million are reported as 0.* For the real data, the three join attributes are time ([days] since January 1st, 1970), latitude ([degrees] between −90 and 90) and longitude ([degrees] between −180 and 180).

Local join algorithm. After partitions are assigned to workers, each worker needs to locally perform a band-join on its partition(s). Many algorithms could be used, ranging from nested-loop to adaptations of IEJoin's sorted arrays and bit-arrays. Since we focus on the *partitioning* aspect, the choice of local implementation is orthogonal, because it only affects the relative importance of optimizing for input duplication vs optimizing for max worker load. We observed that RecPart wins *no matter what this ratio is set to*, therefore

in our experiments we selected a fairly standard local band-join algorithm based on index-nested-loops. (Let S_p and T_p be the input in partition p.) (1) range-partition T_p on A_1 into ranges of size ε_1. (Here A_1 is the most selective dimension.) (2) For each $s \in S_p$, use binary search to find the T-range i containing s. Then check band condition on (s, t) for all t in ranges $(i-1)$, i, and $i+1$.

Since Grid-ε partitions are of size ε_1 in dimension A_1, we slightly modify the above algorithm and sort both S_p and T_p on A_1. The binary search for $s \in S_p$ then searches for $s.A_1 - \varepsilon_1$ (the smallest tuple $t \in T_p$ it could join with) and scans the sorted T-array from there until $s.A_1 + \varepsilon_1$.

Statistics and running-time model. We sample 100,000 input records and set output-sample size so that total time for statistics gathering does not exceed 5% of the fastest time (optimization plus join time) observed for any method. For output sampling we use the method introduced for CS_{IO} [39]. For the cost model (see Section 2), we determine the model coefficients (β-values) as discussed in [25] from a benchmark of 100 queries. The benchmark is run offline once to profile the performance aspects of a cluster.

6.2 Impact of Band Width

We explore the impact of band width, which affects output. For comparison with grid partitioning, we turn RecPart's symmetric partitioning off, i.e., T is always the partitioned/duplicated relation. Since the grid approaches do not apply symmetric partitioning by design, all advantages of RecPart in the experiments are due to the better partition boundaries, not due to symmetric partitioning. (The impact of symmetric partitioning is explored separately later.) To avoid confusion, we refer to RecPart without symmetric partitioning as RecPart-S.

6.2.1 Single Join Attribute. The left block in Table 2a reports running times. *RecPart-S wins in all cases, by up to a factor of 2*, but the other methods are competitive because the join is in 1D and skew is moderate. For CS_{IO} we tried different parameter settings that control optimization time versus partitioning quality, reporting the best found. The right block in Table 2a reports input plus duplicates (I), and the input (I_m) and output (O_m) on the most loaded worker machine. Recall that profiling revealed $\beta_2/\beta_3 \approx 4$, i.e., each input tuple incurs 4 times the load compared to an output tuple.

RecPart-S and CS_{IO} achieve similar load characteristics, because both intelligently leverage input and output samples to balance load while avoiding input duplication. However, RecPart-S finds a better partitioning (lower max worker load and input duplication) with 10x lower optimization time. The other two methods produce significantly higher input duplication, affecting I and I_m. Grid-ε still shows competitive running time because it works with a very fine-grained partitioning, i.e., each worker receives its input already split into many small grid cells. Data in a cell can be joined independent of the other cells, resulting in efficient in-memory processing. As a result, Grid-ε has lower per-tuple processing time than the other methods. (There each worker receives its input in a large "chunk" that needs to be range-partitioned.)

6.2.2 Multiple Join Attributes. Tables 2b and 2c show that the performance gaps widen when joining on 3 attributes: *RecPart-S is the clear winner in total running time as well as join time alone.* It finds the partitioning with the lowest max worker load, while keeping input duplication below 4%, while the competitors created up to 12x input duplication.

CS_{IO} is severely hampered by the complexity of the optimization step. (Lowering optimization time resulted in higher join time due to worse partitioning.) Grid-ε suffers from $O(3^d)$ input duplication in d dimensions. For 1-Bucket, note that the numbers in Table 2a and Table 2b are virtually identical. This is due to the fact that it covers the entire join matrix $S \times T$, i.e., the matrix cover is not affected by the dimensionality of the join condition.

Grid-ε has by far the highest input duplication, but again recovers some of this cost due to its faster local processing that exploits that each worker's input arrives already partitioned into small grid cells. This is especially visible when comparing to 1-Bucket for band width $(2, 2, 2)$ in Table 2c.

6.3 Skew Resistance

Table 3 investigates the impact of join-attribute skew, showing that *RecPart-S handles it the best, again achieving the lowest max worker load with almost no input duplication.* The competitors suffer from high input duplication; CS_{IO} also from high optimization cost. Note that as skew increases, output size increases as well. This is due to the power-law distribution and the correlation of high-frequency join-attribute values in the two inputs. Greater output size implies a denser join matrix for CS_{IO}, increasing its optimization time.

6.4 Scalability

Tables 4a to 4d show that *RecPart-S and RecPart have almost perfect scalability and beat all competitors.* In Tables 4a and 4b, from row to row, we double both input size and number of workers. In Table 4c, only the input size varies while the number of workers is constant. In Table 4d, we only change the number of workers. The latter two results are for an 8D band-join to explore *which techniques can scale beyond dimensionality common today.* For cost reasons, we use the running-time model to predict join time in Tables 4c and 4d. For queries on real data, the smaller inputs are random samples from the full data. Note that join output grows super-linearly, therefore perfect scalability cannot be

Table 2: Impact of band width: RecPart-S wins in all cases, and the winning margin gets bigger for band joins with more dimensions. (Blue color highlights the main results; red color highlights a weak spot.)

(a) `Pareto-`1.5, $d = 1$, varying band width.

Band width	Runtime (optimization time+join time) in [sec]				Relative time over RecPart-S			I/O sizes in [millions]: I, I_m, O_m												
	RecPart-S	CS_{IO}	1-Bucket	Grid-ε	CS_{IO}	1-Bucket	Grid-ε	RecPart-S			CS_{IO}			1-Bucket			Grid-ε		
0	351(3+348)	512(29+483)	762	—	1.46	2.17	N/A	400	14	83	496	13	131	2200	73	81	—	—	—
10^{-5}	539(7+532)	684(29+655)	1004	540	1.27	1.86	1.00	400	12	158	475	8	266	2200	73	153	800	27	153
$2 \cdot 10^{-5}$	813(3+810)	992(30+962)	1316	834	1.22	1.62	1.03	401	13	305	488	10	388	2200	73	304	800	27	304
$3 \cdot 10^{-5}$	878(3+875)	1170(30+1140)	1520	956	1.33	1.73	1.09	401	12	384	479	10	503	2200	73	376	800	27	376

(b) `Pareto-`1.5, $d = 3$, varying band width.

Band width	Runtime (optimization time+join time) in [sec]				Relative time over RecPart-S			I/O sizes in [millions]: I, I_m, O_m												
	RecPart-S	CS_{IO}	1-Bucket	Grid-ε	CS_{IO}	1-Bucket	Grid-ε	RecPart-S			CS_{IO}			1-Bucket			Grid-ε		
(0, 0, 0)	230(1+229)	366(46+320)	792	—	1.59	3.44	N/A	401	14	0	497	17	0	2200	73	0	—	—	—
(2, 2, 2)	344(2+342)	1339(694+645)	1149	1412	3.89	3.34	4.10	404	15	29	652	19	69	2200	73	37	5541	185	37
(4, 4, 4)	860(2+858)	2557(1345+1212)	1772	1816	2.97	2.06	2.11	413	14	290	838	31	321	2200	73	291	5485	183	291

(c) Join of `ebird` with `cloud`, $d = 3$, varying band width.

Band width	Runtime (optimization time+join time) in [sec]				Relative time over RecPart-S			I/O sizes in [millions]: I, I_m, O_m												
	RecPart-S	CS_{IO}	1-Bucket	Grid-ε	CS_{IO}	1-Bucket	Grid-ε	RecPart-S			CS_{IO}			1-Bucket			Grid-ε		
(0, 0, 0)	248(3+245)	346(38+308)	1418	—	1.40	5.72	N/A	890	30	0	951	32	0	4832	161	0	—	—	—
(1, 1, 1)	332(3+329)	1945(968+977)	1532	1419	5.86	4.61	4.27	895	35	5	1490	95	9	4832	161	11	10891	361	11
(2, 2, 2)	423(3+420)	2615(1553+1062)	1573	1377	6.18	3.72	3.26	899	32	66	1830	107	74	4832	161	67	10783	361	74

Table 3: Skew resistance: RecPart-S is fastest and has much less data duplication than other methods. (`Pareto-`z, $d = 3$, band width $(2, 2, 2)$, and increasing skew $z = 0.5, \ldots, 2$.)

Data Sets	Runtime (optimization time+join time) in [sec]				Relative time over RecPart-S			I/O sizes in [millions]: I, I_m, O_m												
	RecPart-S	CS_{IO}	1-Bucket	Grid-ε	CS_{IO}	1-Bucket	Grid-ε	RecPart-S			CS_{IO}			1-Bucket			Grid-ε		
`pareto-0.5`	230 (3+227)	609 (263+346)	1137	1146	2.65	4.94	4.98	401	13	0.3	577	20	1	2200	73	0.4	5582	186	0.4
`pareto-1.0`	290 (3+287)	1064 (525+539)	1235	1335	3.67	4.26	4.60	401	13	17	616	20	31	2200	73	14	5554	185	14
`pareto-1.5`	344 (2+342)	1339 (694+645)	1149	1412	3.89	3.34	4.10	404	15	29	652	19	69	2200	73	37	5541	185	37
`pareto-2.0`	485 (2+483)	1811 (1000+811)	1369	2417	3.73	2.82	4.98	406	14	111	747	19	168	2200	73	107	5522	184	107

achieved. Nevertheless, RecPart-S and RecPart come close to the ideal when taking the output increase into account. When the same query is run on different-sized clusters (Table 4d), RecPart scales out best. CS_{IO}'s optimization time grows substantially as w increases. We explored various settings, but reducing optimization time resulted in even higher join time and vice versa. The numbers shown represent the best tradeoff found. Grid-ε failed on the largest synthetic input due to a memory exception caused by one of the grid cells receiving too many input records.

6.5 Optimizing Grid Size

Table 5 shows that grid granularity has a significant impact on join time, here model estimated, of Grid-ε. With the default grid size $(2, 2, 2)$, join time is 9x higher compared to grid size $(32, 32, 32)$, caused by input duplication. Our extension *Grid* automatically explores different grid sizes*, using the same running-time model $\mathcal{M}$ as RecPart and CS_{IO} to find the best setting. Starting with grid size ε_i in dimension i for all join attributes A_i, it tries coarsening the grid to size $j \cdot \varepsilon_i$ in dimension i, for $j = 2, 3, \ldots$ For each resulting grid partitioning $\mathcal{G}$, we execute $\mathcal{M}(\mathcal{G})$ to let model $\mathcal{M}$ predict the running time, until a local minimum is found.

Automatic grid tuning works well for `Pareto-`z where both inputs are similarly distributed and band width is small: Lemma 3 applies with large c_1 and small c_2, providing strong upper bounds on the amount of input in any ε-range. This confirms that grid-partitioning can indeed work well for "sufficiently large" input even in 3D space. However, Grid* fails on the reverse Pareto distribution as Table 6 shows. There S and T have very different density, resulting in small c_1 and large c_2, and therefore much weaker upper bounds on the input per ε-range. The resulting dense regions, as stated by Lemma 2, cause high input duplication and high input I_m assigned to the most loaded worker.

6.6 Comparing to Distributed IEJoin

Table 7 shows representative results for a comparison to the quantile-based partitioning used by IEJoin [19]. We explore a wide range of inter-quantile ranges (sizePerBlock) and report results for those at and near the best setting found. Note that RecPart can use the same local processing algorithm as IEJoin, therefore we are interested in comparing based on *the quality of the partitioning*, i.e., I, I_m, and O_m. It is clearly visible that *RecPart-S finds significantly better partitionings*, providing more evidence that simple quantile-based partitioning of the join matrix does not suffice.

Table 4: Scalability experiments: RecPart-S and RecPart have almost perfect scalability and beat all competitors. (Dataset $X/Y/w$ in (a) and (b) refers to X million input and Y million output on w workers.)

(a) `Pareto-1.5`, $d = 3$, band width $(2, 2, 2)$.

Data Sets	Runtime (optimization time+join time) in [sec]				Relative time over RecPart-S			I/O sizes in [millions]: I, I_m, O_m												
	RecPart-S	CS_{IO}	1-Bucket	Grid-ε	CS_{IO}	1-Bucket	Grid-ε	RecPart-S			CS_{IO}			1-Bucket			Grid-ε		
200/282/15	306 (1+305)	1227 (767+460)	779	1381	4.01	2.55	4.51	202	13	20	290	19	36	800	53	19	2772	185	19
400/1120/30	344 (2+342)	1374 (729+645)	1149	1412	3.99	3.34	4.10	404	15	29	652	19	69	2200	73	37	5541	185	37
800/4460/60	438 (4+434)	1721 (801+920)	1731	FAILED	3.93	3.95	N/A	809	21	45	1690	42	74	6400	107	74	11089	185	74

(b) Join of `ebird` with `cloud`, $d = 3$, band width $(2, 2, 2)$.

Data Sets	Runtime (optimization time+join time) in [sec]				Relative time over RecPart-S			I/O sizes in [millions]: I, I_m, O_m												
	RecPart-S	CS_{IO}	1-Bucket	Grid-ε	CS_{IO}	1-Bucket	Grid-ε	RecPart-S			CS_{IO}			1-Bucket			Grid-ε		
222/134/15	207 (3+204)	1213 (942+271)	547	812	5.86	2.64	3.92	223	15	11	307	22	11	856	57	9	2688	179	9
445/530/30	193 (3+190)	1778 (1447+331)	688	771	9.21	3.56	3.99	448	16	14	748	26	27	2420	81	18	5403	180	18
890/2000/60	215 (2+213)	1919 (1479*+440)	1117	793	8.93	5.20	3.69	899	13	44	2040	38	35	6870	114	36	10805	180	36

* optimization time for 890/2000/60 is similar to that of 445/530/30 after we tuned parameters for CS_{IO} s.t. it could finish optimization within 90 minutes.

(c) Varying input size: `pareto-1.5`, $d = 8$, band width is 20 in each dimension, 30 workers.

Input Size in [millions]	Join Result Size in [millions]	Runtime (optimization time+join time) in [sec]				I/O sizes in [millions]: I, I_m, O_m											
		RecPart	CS_{IO}	1-Bucket	Grid-ε	RecPart			CS_{IO}			1-Bucket			Grid-ε		
100	9	61 (5+56)	528 (449+79)	292	173,581	104	3	2	142	5	1	550	18	0.3	297,421	9,914	0.3
200	57	120 (5+115)	612 (448+164)	587	347,944	210	7	2	285	10	5	1100	37	2	594,834	19,828	2
400	219	240 (8+232)	760 (418+342)	1180	694,574	420	14	7	574	7	67	2200	73	7	1,189,996	39,667	7
800	857	510 (17+493)	1166 (423+743)	2390	$1.39 \cdot 10^6$	847	26	31	1180	53	4	4400	147	29	2,379,329	79,311	29

(d) Varying number of workers (w): `pareto-1.5`, $d = 8$, band width is 20 in each dimension, input size 400 million.

w	Join Result Size in [millions]	Runtime (optimization time+join time) in [sec]				I/O sizes in [millions]: I, I_m, O_m											
		RecPart	CS_{IO}	1-Bucket	Grid-ε	RecPart			CS_{IO}			1-Bucket			Grid-ε		
1	219	3655	3655	3655	8,527,502	400	400	219	400	400	219	400	400	219	1,189,996	1,189,996	219
15		358 (5+353)	710 (190+520)	1295	1,040,000	420	28	10	565	40	29	1600	107	15	1,189,996	79,333	15
30		240 (8+232)	760 (418+342)	1180	695,000	420	14	7	574	7	67	2200	73	7	1,189,996	39,667	7
60		182 (10+172)	3703 (3431+272)	1287	525,000	425	6	5	619	13	2	3200	53	4	1,189,996	19,833	4

Table 5: Grid-ε vs. Grid* on `pareto-`1.5, band width $(2, 2, 2)$, varying grid size (I, I_m and O_m in [millions]).

Grid-ε				
Grid Size	I	I_m	O_m	Join Time
(1,1,1)	5610	180	38	2993
(2,2,2)	5541	185	37	3021
(4,4,4)	1780	60	38	1023
(8,8,8)	861	29	38	533
(16,16,16)	582	20	39	389
(32,32,32)	478	16	42	336
(64,64,64)	435	15	56	344

	I	I_m	O_m	Join Time
Grid*	460	16	46	335
RecPart-S	404	15	29	286
CS_{IO}	652	19	69	459
1-Bucket	2200	73	37	1236

Table 6: Grid* vs. RecPart. I/O sizes in [millions].

Data Sets	Band width	RecPart			Grid*			
		I	I_m	O_m	Grid Size	I	I_m	O_m
`pareto-2.0`	(2,2,2)	406	14	111	8	497	17	130
`rv-pareto-1.5`	(1K,1K,1K)	400	13	0	2750	882	237	0
`rv-pareto-1.5`	(2K,2K,2K)	401	13	0	11500	1207	401	0

6.7 Impact of Local Join Algorithm

Table 8 shows a typical result of the impact of ratio β_2/β_1. A high ratio occurs in systems with fast data transfer and slow local computation. Replacing the local band-join algorithm with a faster one would lower the ratio. While the competitors are not affected by the ratio (they all ignore network shuffle time), it is visible how *increasing weight on local join cost makes RecPart reduce max worker load*, incurring slightly higher input duplication.

Table 7: Comparing to distributed IEJoin: Input duplication and max worker load on `pareto-`z, $w = 30$, varying skew and band width (I, I_m and O_m in [millions]).

Z	Band width	Output size	RecPart-S			IEJoin			
			I	I_m	O_m	I	I_m	O_m	sizePerBlock
1.5	[0,0,0]	0	401	14	0	780	40	0	10000
						726	25	0	12524
						756	28	0	14000
1.5	[2,2,2]	1120	404	15	29	1092	48	14	6000
						1070	45	21	7422
						1062	36	85	9000
1.0	[2,2,2]	420	401	13	17	1176	40	21	4000
						1080	37	26	6263
						1088	48	4	8000
0.5	[2,2,2]	12	401	13	0.3	828	24	1	6000
						796	17	2	8295
						820	20	2	10000

6.8 Impact of Symmetric Partitioning

While RecPart and RecPart-S find similar partitionings on `pareto-1.0` and the real data, the advantages of symmetric partitioning are revealed on the reverse Pareto data in Table 9. Here RecPart-S cannot split regions with high density of T without incurring high input duplication. In

Table 8: Impact of local join algorithm: Input duplication I vs max worker load $L_m = 4I_m + O_m$ for varying ratios β_2/β_1 for join of `ebird` with `cloud`, band width $(2, 2, 2)$, $w = 30$.

β_2/β_1	RecPart		CS_{IO}		1-Bucket		Grid-ε	
	I	L_m	I	L_m	I	L_m	I	L_m
0.0001	890.34	289						
0.001	890.36	223						
0.01	890.42	195						
0.1	890.52	191						
1	890.8	189	1830	502	4832	711	10800	1518
10	890.8	189						
100	890.8	189						
1000	890.8	189						
10000	890.8	189						

Table 9: RecPart-S vs. RecPart (I/O sizes in [millions]).

Data Sets	Band width	RecPart-S			RecPart		
		I	I_m	O_m	I	I_m	O_m
`pareto-1.0`	(2,2,2)	401	13	17	401	12	21
`ebird` and `cloud`	(0,0,0)	890	30	0	890	30	0
`ebird` and `cloud`	(2,2,2)	899	32	66	891	31	67
`ebird` and `cloud`	(4,4,4)	918	31	567	894	30	515
`rv-pareto-1.5`	(1000,1000,1000)	452	143	0	400	13	0
`rv-pareto-1.5`	(2000,2000,2000)	430	173	0	401	13	0
`rv-pareto-1.5`	2	433	40	0	401	14	0
`rv-pareto-1.5`	1000	402	200	0	402	14	0

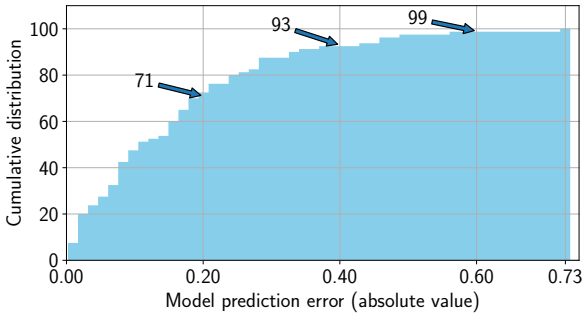

Figure 9: Accuracy of the running-time model: Cumulative distribution of model error.

contrast, RecPart switches the roles of S and T, because S is sparse in those regions and hence the split creates few input duplicates.

6.9 Accuracy of the Running-Time Model

In all experiments, the running-time model's predictions were sufficiently accurate for identifying excellent partitionings for RecPart. Due to the high cost in terms of time and money of executing computations in the cloud, we sometimes rely on the running-time model also to report join time. Figure 9 shows the cumulative distribution of the relative error between predicted and measured join time for over 80 experiments selected randomly from all runs. E.g., the model has less than 20% error in over 70% of the cases and it is never off by more than a factor 1.8.

6.10 Near-Optimality of Our Approach

Figure 4 in Section 1 summarizes the results from all tables, making it easy to see how RecPart achieves significantly lower max worker load (y-axis) with less input duplication (x-axis). RecPart is always within 10% of the lower bound on both measures, beating the competition by a wide margin.

7 CONCLUSIONS

For distributed band-joins, we showed that recursive partitioning with the appropriate split-scoring measure achieves both low optimization time (a few seconds) and near-optimal join partitioning (within 10% of the respective lower bounds) on input duplication and max worker load. Even if system parameters change, e.g., due to faster networks or CPUs, RecPart's achievement will still stand, because the issues of low input duplication and low input and output per worker will remain crucial optimization goals.

There are several exciting directions for future work. First, for band-joins between more than two relations, can one do better than reducing the problem to multiple two-way joins? Second, how do we partition for join conditions that contain a mix of various types of predicates, e.g., equality, inequality, band, and non-equality? Third, what other types of join conditions give rise to specialized methods, like RecPart for band-join, so that similarly significant improvements over generic theta-join approaches can be achieved?

More information about RecPart and other techniques for distributed data-intensive computations can be found at https://northeastern-datalab.github.io/distributed/.

ACKNOWLEDGMENTS

This work was supported in part by the National Institutes of Health (NIH) under award number R01 NS091421 and by the National Science Foundation (NSF) under award number CAREER IIS-1762268. The content is solely the responsibility of the authors and does not necessarily represent the official views of NIH or NSF. We also would like to thank Aditya Ghosh for his contributions to the design and implementation of Grid*, Dhavalkumar Patel for implementing the join-sampling algorithm, and the anonymous reviewers and Niklas Smedemark-Margulies for their constructive feedback.

REFERENCES

[1] Paul Beame, Paraschos Koutris, and Dan Suciu. 2014. Skew in parallel query processing. In *PODS*. 212–223. https://doi.org/10.1145/2594538.2594558

[2] Carsten Binnig, Andrew Crotty, Alex Galakatos, Tim Kraska, and Erfan Zamanian. 2016. The End of Slow Networks: It's Time for a Redesign. *PVLDB* 9, 7 (2016), 528–539. https://doi.org/10.14778/2904483.2904485

[3] Spyros Blanas, Jignesh M Patel, Vuk Ercegovac, Jun Rao, Eugene J Shekita, and Yuanyuan Tian. 2010. A comparison of join algorithms for log processing in mapreduce. In *SIGMOD*. 975–986. https://doi.org/10.1145/1807167.1807273

[4] Nicolas Bruno, YongChul Kwon, and Ming-Chuan Wu. 2014. Advanced join strategies for large-scale distributed computation. *PVLDB* 7, 13 (2014), 1484–1495. https://doi.org/10.14778/2733004.2733020

[5] Shumo Chu, Magdalena Balazinska, and Dan Suciu. 2015. From theory to practice: Efficient join query evaluation in a parallel database system. In *SIGMOD*. 63–78. https://doi.org/10.1145/2723372.2750545

[6] Jeffrey Dean and Sanjay Ghemawat. 2008. MapReduce: Simplified Data Processing on Large Clusters. *Commun. ACM* 51, 1 (2008), 107–113. https://doi.org/10.1145/1327452.1327492

[7] Hasanat M Dewan, Kui W Mok, Mauricio Hernández, and Salvatore J Stolfo. 1994. Predictive dynamic load balancing of parallel hash-joins over heterogeneous processors in the presence of data skew. In *PDIS*. 40–49. https://doi.org/10.1109/PDIS.1994.331734

[8] David J DeWitt and Robert Gerber. 1985. Multiprocessor hash-based join algorithms. In *VLDB*. 151–164. https://dl.acm.org/doi/10.5555/1286760.1286774

[9] David J DeWitt, Jeffrey F Naughton, and Donovan A Schneider. 1991. An evaluation of non-equijoin algorithms. In *VLDB*. 443–452. https://dl.acm.org/doi/10.5555/645917.672320

[10] David J DeWitt, Jeffrey F Naughton, Donovan A Schneider, and Srinivasan Seshadri. 1992. Practical skew handling in parallel joins. In *VLDB*. 27–40. https://dl.acm.org/doi/10.5555/645918.672512

[11] Jennie Duggan, Olga Papaemmanouil, Leilani Battle, and Michael Stonebraker. 2015. Skew-aware join optimization for array databases. In *SIGMOD*. 123–135. https://doi.org/10.1145/2723372.2723709

[12] Mohammed Elseidy, Abdallah Elguindy, Aleksandar Vitorovic, and Christoph Koch. 2014. Scalable and adaptive online joins. *PVLDB* 7, 6 (2014), 441–452. https://doi.org/10.14778/2732279.2732281

[13] Fabian Fier, Nikolaus Augsten, Panagiotis Bouros, Ulf Leser, and Johann-Christoph Freytag. 2018. Set Similarity Joins on MapReduce: An Experimental Survey. *PVLDB* 11, 10 (2018), 1110–1122. https://doi.org/10.14778/3231751.3231760

[14] Paula Furtado and Peter Baumann. 1999. Storage of Multidimensional Arrays Based on Arbitrary Tiling. In *ICDE*. 480–489. https://doi.org/10.1109/ICDE.1999.754964

[15] CJ Hahn, SG Warren, and R Eastman. 2012. Extended Edited Synoptic Cloud Reports from Ships and Land Stations Over the Globe, 1952-2009 (NDP-026C). (2012). https://doi.org/10.3334/CDIAC/cli.ndp026c

[16] Jiawei Han, Jian Pei, and Micheline Kamber. 2011. *Data mining: concepts and techniques* (3rd ed.). Morgan Kaufmann. https://doi.org/10.1016/C2009-0-61819-5

[17] Lilian Harada and Masaru Kitsuregawa. 1995. Dynamic Join Product Skew Handling for Hash-Joins in Shared-Nothing Database Systems.. In *DASFAA*. 246–255. https://dl.acm.org/doi/10.5555/646710.703010

[18] Kien A Hua and Chiang Lee. 1991. Handling Data Skew in Multiprocessor Database Computers Using Partition Tuning. In *VLDB*. 525–535. https://dl.acm.org/doi/10.5555/645917.672154

[19] Zuhair Khayyat, William Lucia, Meghna Singh, Mourad Ouzzani, Paolo Papotti, Jorge-Arnulfo Quiané-Ruiz, Nan Tang, and Panos Kalnis. 2017. Fast and scalable inequality joins. *VLDBJ* 26, 1 (2017), 125–150. https://doi.org/10.1007/s00778-016-0441-6

[20] Masaru Kitsuregawa and Yasushi Ogawa. 1990. Bucket Spreading Parallel Hash: A New, Robust, Parallel Hash Join Method for Data Skew in the Super Database Computer (SDC). In *VLDB*. 210–221. https://dl.acm.org/doi/10.5555/94362.94416

[21] Masaru Kitsuregawa, Hidehiko Tanaka, and Tohru Moto-Oka. 1983. Application of hash to data base machine and its architecture. *New Generation Computing* 1, 1 (1983), 63–74. https://doi.org/10.1007/BF03037022

[22] Ioannis Koumarelas, Athanasios Naskos, and Anastasios Gounaris. 2018. Flexible Partitioning for Selective Binary Theta-joins in a Massively Parallel Setting. *Distrib. Parallel Databases* 36, 2 (2018), 301–337. https://doi.org/10.1007/s10619-017-7214-0

[23] Usha Krishnamurthy. 2019. *Oracle Database SQL Language Reference 19c*. Oracle. https://docs.oracle.com/en/database/oracle/oracle-database/19/sqlrf/index.html Version 19.1.

[24] Rundong Li, Wolfgang Gatterbauer, and Mirek Riedewald. 2020. Near-Optimal Distributed Band-Joins through Recursive Partitioning. (2020). arXiv:cs.DB/2004.06101

[25] Rundong Li, Ningfang Mi, Mirek Riedewald, Yizhou Sun, and Yi Yao. 2019. Abstract cost models for distributed data-intensive computations. *Distrib.Parallel Databases* 37, 3 (2019), 411–439. https://doi.org/10.1007/s10619-018-7244-2

[26] Rundong Li, Mirek Riedewald, and Xinyan Deng. 2018. Submodularity of Distributed Join Computation. In *SIGMOD*. 1237–1252. https://doi.org/10.1145/3183713.3183728

[27] HJ Lu and Kian-Lee Tan. 1994. Load-balanced join processing in shared-nothing systems. *J. Parallel and Distrib. Comput.* 23, 3 (1994), 382–398. https://doi.org/10.1006/jpdc.1994.1148

[28] Arthur M Munson, Kevin Webb, Daniel Sheldon, Daniel Fink, Wesley M Hochachka, Marshall Iliff, Mirek Riedewald, Daria Sorokina, Brian Sullivan, Christopher Wood, and Steve Kelling. 2014. The ebird reference dataset, version 2014. *Cornell Lab of Ornithology and National Audubon Society, Ithaca, NY* (2014). https://ebird.org

[29] Alper Okcan and Mirek Riedewald. 2011. Processing Theta-joins Using MapReduce. In *SIGMOD*. 949–960. https://doi.org/10.1145/1989323.1989423

[30] Orestis Polychroniou, Rajkumar Sen, and Kenneth A Ross. 2014. Track join: distributed joins with minimal network traffic. In *SIGMOD*. 1483–1494. https://doi.org/10.1145/2588555.2610521

[31] Viswanath Poosala and Yannis E Ioannidis. 1996. Estimation of query-result distribution and its application in parallel-join load balancing. In *VLDB*. 448–459. https://dl.acm.org/doi/10.5555/645922.673321

[32] Viswanath Poosala and Yannis E Ioannidis. 1997. Selectivity estimation without the attribute value independence assumption. In *VLDB*. 486–495. https://dl.acm.org/doi/10.5555/645923.673638

[33] Viswanath Poosala, Yannis E. Ioannidis, Peter J. Haas, and Eugene J. Shekita. 1996. Improved Histograms for Selectivity Estimation of Range Predicates. In *SIGMOD*. 294–305. https://doi.org/10.1145/233269.233342

[34] Wolf Rödiger, Sam Idicula, Alfons Kemper, and Thomas Neumann. 2016. Flow-join: Adaptive skew handling for distributed joins over high-speed networks. In *ICDE*. 1194–1205. https://doi.org/10.1109/ICDE.2016.7498324

[35] Akash Das Sarma, Yeye He, and Surajit Chaudhuri. 2014. ClusterJoin: A Similarity Joins Framework using Map-Reduce. *PVLDB* 7, 12 (2014), 1059–1070. https://doi.org/10.14778/2732977.2732981

[36] Donovan A Schneider and David J DeWitt. 1989. A performance evaluation of four parallel join algorithms in a shared-nothing multiprocessor environment. In *SIGMOD*. 110–121. https://doi.org/10.1145/67544.66937

[37] Donovan A Schneider and David J DeWitt. 1990. Tradeoffs in processing complex join queries via hashing in multiprocessor database machines. In *VLDB*. 469–480. https://dl.acm.org/doi/10.5555/645916.672141

[38] Valery Soloviev. 1993. A truncating hash algorithm for processing band-join queries. In *ICDE*. 419–427. https://doi.org/10.1109/ICDE.1993.344039

[39] Aleksandar Vitorovic, Mohammed Elseidy, and Christoph Koch. 2016. Load balancing and skew resilience for parallel joins. In *ICDE*. 313–324.

https://doi.org/10.1109/ICDE.2016.7498250

[40] Christopher B Walton, Alfred G Dale, and Roy M Jenevein. 1991. A Taxonomy and Performance Model of Data Skew Effects in Parallel Joins.. In *VLDB*. 537–548. https://dl.acm.org/doi/10.5555/645917.672307

[41] Joel L. Wolf, Daniel M. Dias, Philip S. Yu, and John Turek. 1994. New algorithms for parallelizing relational database joins in the presence of data skew. *TKDE* (1994), 990–997. https://doi.org/10.1109/69.334888

[42] Yu Xu, Pekka Kostamaa, Xin Zhou, and Liang Chen. 2008. Handling data skew in parallel joins in shared-nothing systems. In *SIGMOD*. 1043–1052. https://doi.org/10.1145/1376616.1376720

[43] Matei Zaharia, Mosharaf Chowdhury, Michael J Franklin, Scott Shenker, and Ion Stoica. 2010. Spark: cluster computing with working sets. In *USENIX HotCloud*. https://dl.acm.org/doi/10.5555/1863103.1863113

[44] Xiaofei Zhang, Lei Chen, and Min Wang. 2012. Efficient Multi-way Theta-join Processing Using MapReduce. *PVLDB* 5, 11 (2012), 1184–1195. https://doi.org/10.14778/2350229.2350238

[45] Weijie Zhao, Florin Rusu, Bin Dong, and Kesheng Wu. 2016. Similarity Join over Array Data. In *SIGMOD*. 2007–2022. https://doi.org/10.1145/2882903.2915247